Nuclear Engineering and Technology 51 (2019) 654–664

Contents lists available at ScienceDirect

Nuclear Engineering and Technology

journal homepage: www.elsevier.com/locate/net

Original Article

# Mathematical approach for optimization of magnetohydrodynamic circulation system

Geun Hyeong Lee, Hee Reyoung Kim*

*Ulsan National Institute of Science and Technology, Department of Nuclear Engineering, Ulsan, 689-798, Republic of Korea*

ARTICLE INFO

*Article history:*
Received 13 September 2018
Received in revised form
3 November 2018
Accepted 12 December 2018
Available online 13 December 2018

*Keywords:*
Magnetohydrodynamics (MHD)
Rectangular-type circulation system
Magnetic flux density
Current

ABSTRACT

The geometrical and electromagnetic variables of a rectangular-type magnetohydrodynamic (MHD) circulation system are optimized to solve MHD equations for the active decay heat removal system of a prototype Gen-IV sodium fast reactor. Decay heat must be actively removed from the reactor coolant to prevent the reactor system from exceeding its temperature limit. A rectangular-type MHD circulation system is adopted to remove this heat via an active system that produces developed pressure through the Lorentz force of the circulating sodium. Thus, the rectangular-type MHD circulation system for a circulating loop is modeled with the following specifications: a developed pressure of 2 kPa and flow rate of 0.02 $m^3/s$ at a temperature of 499 K. The MHD equations, which consist of momentum and Maxwell's equations, are solved to find the minimum input current satisfying the nominal developed pressure and flow rate according to the change of variables including the magnetic flux density and geometrical variables. The optimization shows that the rectangular-type MHD circulation system requires a current of 3976 A and a magnetic flux density of 0.037 T under the conditions of the active decay heat removal system.



## 1. Introduction

Magnetohydrodynamic (MHD) circulation systems are used to circulate liquid metals because they do not have sealing and rotational/moving parts, eliminating the possibility of liquid-metal leakage. A rectangular-type MHD circulation system was previously considered for the active decay heat removal system (ADHRS) used to transport liquid sodium coolant to a prototype Gen-IV sodium fast reactor (PGSFR). The MHD circulation system of the ADHRS uses an electromagnetic force (according to the Lorentz force principle) for circulating liquid sodium in the loop system. The loop contains a blower with a finned-tube sodium-to-air heat exchanger (FDHX), as shown in Fig. 1. A rectangular-type MHD circulation system was considered for circulating liquid sodium because of its high electrical conductivity, which can be used to generate Lorentz force from the vector product of the current density (J) and magnetic field (B) [1].

In the present study, a mathematical approach to model the rectangular MHD circulation system is implemented, and the corresponding MHD equations are solved by means of a numerical analysis method for calculating electromagnetic force. The approach is focused on the optimization analysis of magnetic flux density and current for the developed pressure generated from Lorentz force. Moreover, the pressure loss produced by hydraulic and force due to electromotive was analyzed using the geometrical variables of the MHD circulation system [2,3]. We determined the variables for the minimum input current by using pressure calculations and analyzed the numerical values for the model optimization of the MHD circulation system.

## 2. Analysis of rectangular-type MHD circulation system

An MHD circulation system contains three components: a permanent magnet, an electrode stub, and a system duct, and its mathematical model is shown in Fig. 2. A Lorentz force is generated and can be calculated from the vector product of the electrode stub current [4] and the magnetic flux density of the permanent magnet [5,6]. The circulation system is based on the MHD principle, which requires the solution of Maxwell's equation of Ampere's law, Faraday's law, Gauss's law for magnetism, Ohm's law, and the Navier–Stokes equation, as expressed in Equations (1)–(5).

* Corresponding author.
*E-mail address:* kimhr@unist.ac.kr (H.R. Kim).

https://doi.org/10.1016/j.net.2018.12.008

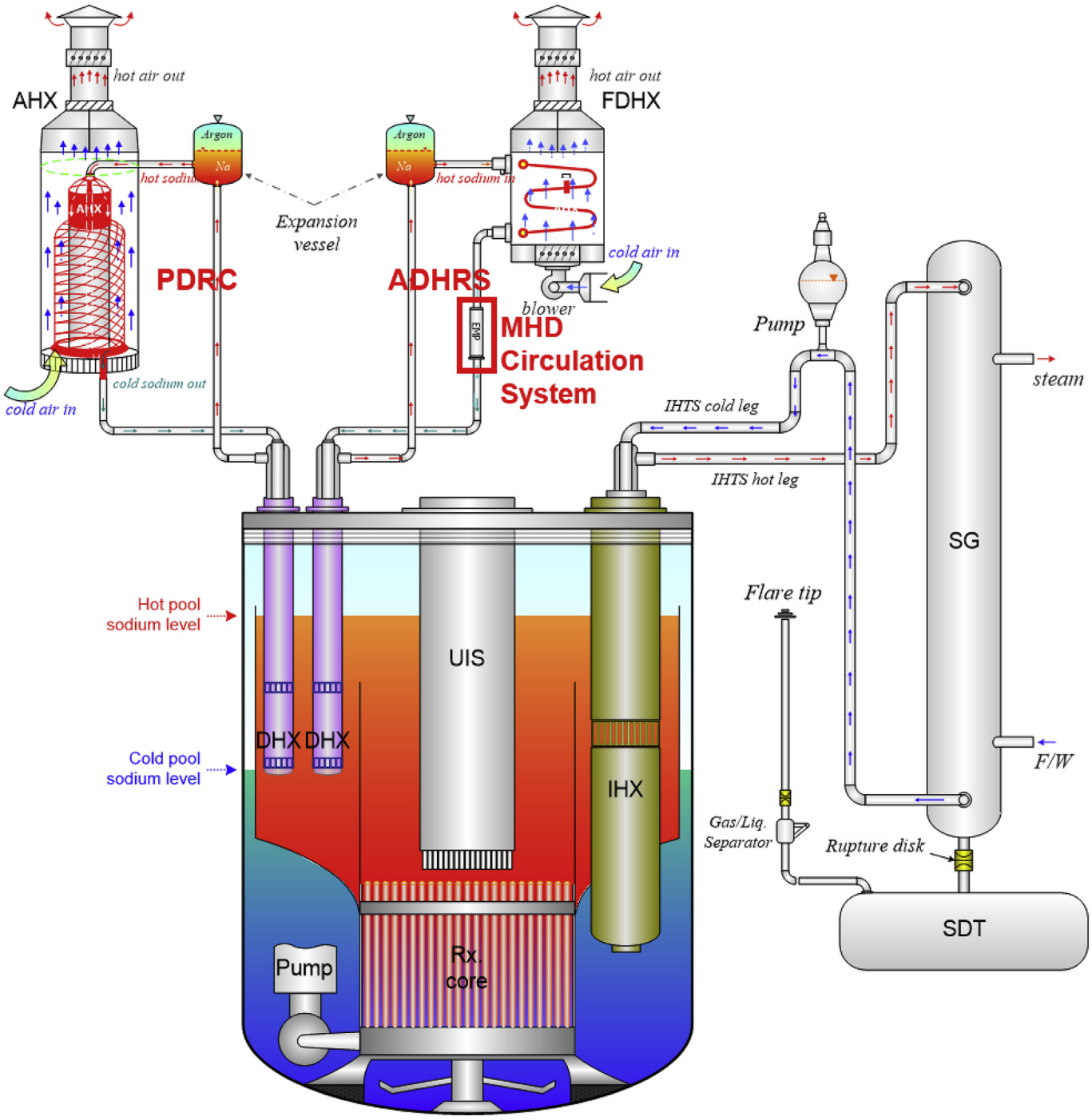


**Fig. 1.** Schematic of the PGSFR

$$\text{Ampere's law: } \nabla \times \vec{B} = \mu_0\left(\vec{J} + \varepsilon_0\frac{\partial \vec{E}}{\partial t}\right) \quad (1)$$

$$\text{Faraday's law: } \nabla \times \vec{E} = -\frac{\partial \vec{B}}{\partial t} \quad (2)$$

$$\text{Gauss's law for magnetism: } \nabla \cdot \vec{B} = 0 \quad (3)$$

$$\text{Ohm's law: } \vec{J} = \sigma(\vec{E} + \vec{v} \times \vec{B}) \quad (4)$$

$$\text{Navier} - \text{Stokes equation: } \frac{\partial \vec{v}}{\partial t} + (\vec{v}\cdot\nabla)\vec{v} = -\frac{1}{\rho}\nabla\left(\vec{p} + \vec{p_h}\right) + \nu\nabla^2\vec{v} + \frac{1}{\rho}\vec{J_t} \times \vec{B} \quad (5)$$

The relationships between magnetic flux density and pressures which is generated by vector product of current flowing through electric stub and external magnetic flux density from permanent

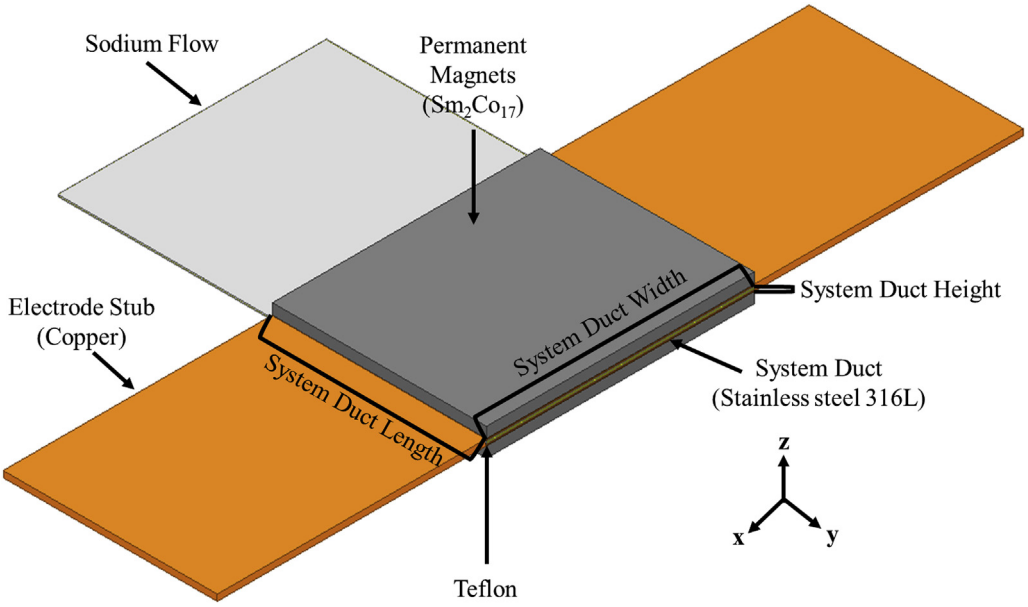


**Fig. 2.** Schematic of the rectangular-type MHD circulation system.

magnet are analyzed solving MHD equations. The magnetic flux densities at liquid sodium flow channel depend on both the induced magnetic field from electrode stub and external magnetic field from permanent magnet. The developed pressure is determined solving Navier-Stokes equation including Lorentz force ($\vec{J_t} \times \vec{B}$) as an external force term in Equation (5).

The components of electric field, current density, magnetic flux density, and fluid velocity are represented in Equations (6)-(11) in a Cartesian coordinate system [7]. The $z$-direction electric field of the MHD circulation system is negligible because of the nonconductive material (Teflon) between the permanent magnet and system duct. This prevents current from flowing to the permanent magnet, as well as the narrow flow channel gap in Equation (6) for the increasing current flowing in liquid sodium. The rotating electrons of the permanent magnet create a magnetic field [8]. The microscopic circulating current in the permanent magnet is negligible in terms of analyzing the induced current of system. Therefore, the magnetic flux density is divided into the external one from the permanent magnet and the one induced by the electrode-stub current density, as described in Equation (8) [9,10]. Only the $y$-direction fluid velocity is considered, as expressed in Equation (11).

$$\vec{E}_t(x,y,z) = E_x\hat{x} + E_y\hat{y} \tag{6}$$

$$\vec{J}_t(x,y,z) = J_x\hat{x} + J_y\hat{y} + J_z\hat{z} \tag{7}$$

$$\vec{B}_t(x,y,z) = \vec{B}_e(x,y,z) + \vec{B}_n(x,y,z) \tag{8}$$

$$\vec{B}_e(x,y,z) = B_{e,x}\hat{x} + B_{e,y}\hat{y} + B_{e,z}\hat{z} \tag{9}$$

$$\vec{B}_i(x,y,z) = B_{i,x}\hat{x} + B_{i,y}\hat{y} + B_{i,z}\hat{z} \tag{10}$$

$$\vec{v}(x,y,z) = v_y\hat{y} \tag{11}$$

Ampere's law in Equation (1) is represented as Equations (12)-(15), using the curl operator in Cartesian coordinates. Here, the time-varying term is negligible because the MHD circulation system employs a direct current source. The external magnetic flux density is negligible because it is affected by the circulating current in the permanent magnet. Therefore, only the induced magnetic flux density is affected by the current density.

$$\nabla \times \vec{B}_n = \mu_0 \vec{J}_t \tag{12}$$

$$\nabla \times \vec{B}_i = \left(\frac{\partial B_{n,z}}{\partial y} - \frac{\partial B_{n,y}}{\partial z}\right)\hat{x} + \left(\frac{\partial B_{n,x}}{\partial z} - \frac{\partial B_{n,z}}{\partial x}\right)\hat{y} + \left(\frac{\partial B_{n,y}}{\partial x} - \frac{\partial B_{n,x}}{\partial y}\right)\hat{z} \tag{13}$$

$$\mu_0 \vec{J}_t = \mu_0\left(J_x\hat{x} + J_y\hat{y} + J_z\hat{z}\right) \tag{14}$$

$$\frac{\partial B_{n,z}}{\partial y} - \frac{\partial B_{n,y}}{\partial z} = \mu_0 J_x,\ \frac{\partial B_{n,x}}{\partial z} - \frac{\partial B_{n,z}}{\partial x} = \mu_0 J_y,\ \frac{\partial B_{n,y}}{\partial x} - \frac{\partial B_{n,x}}{\partial y} = \mu_0 J_z \tag{15}$$

Faraday's law in Equation (2) is represented as Equations (16)-(18) by using the curl operator in Cartesian coordinates, where the time-varying term vanished because of the direct current source and permanent magnet.

$$\nabla \times \vec{E}_t = 0 \tag{16}$$

$$\nabla \times \vec{E}_t = -\frac{\partial E_y}{\partial z}\hat{x} + \frac{\partial E_x}{\partial z}\hat{y} + \left(\frac{\partial E_y}{\partial x} - \frac{\partial E_x}{\partial y}\right)\hat{z} \tag{17}$$

$$\frac{\partial E_y}{\partial z} = 0, \frac{\partial E_x}{\partial z} = 0, \frac{\partial E_y}{\partial x} - \frac{\partial E_x}{\partial y} = 0 \tag{18}$$

Gauss's law for magnetism in Equation (3) is expressed using a divergence operator in Cartesian coordinates, as described by Equations (19)-(22). The divergence of external and internal magnetic flux density becomes zero.

$$\nabla\cdot\vec{B}_e = 0 \tag{19}$$

$$\nabla\cdot\vec{B}_i = 0 \tag{20}$$

$$\nabla\cdot\vec{B}_e = \frac{\partial(B_{e,x})}{\partial x} + \frac{\partial(B_{e,y})}{\partial y} + \frac{\partial(B_{e,z})}{\partial z} = 0 \tag{21}$$

$$\nabla\cdot\vec{B}_i = \frac{\partial(B_{n,x})}{\partial x} + \frac{\partial(B_{n,y})}{\partial y} + \frac{\partial(B_{n,z})}{\partial z} = 0 \tag{22}$$

Ohm's law in Equation (4) is expressed by Equations (23)-(26) using the vector product of velocity and magnetic flux density.

$$\vec{J}_t = \sigma(\vec{E}_t + \vec{v}\times\vec{B}_t) \tag{23}$$

$$\vec{J}_t = J_x\hat{x} + J_y\hat{y} + J_z\hat{z} \tag{24}$$

$$\sigma(\vec{E}_t + \vec{v}\times\vec{B}_t) = \sigma\{(E_x + v_yB_{n,z} + v_yB_{e,z})\hat{x} + E_y\hat{y} - (v_yB_{n,x} - v_yB_{e,x})\hat{z}\} \tag{25}$$

$$J_x = \sigma(E_x + v_yB_{n,z} + v_yB_{e,z}), J_y = \sigma E_y, J_z = \sigma(v_yB_{n,x} - v_yB_{e,x}) \tag{26}$$

The summation from Equations (15) and (22) can eliminate the current density, and the electric field is eliminated by Equation (18). Therefore, the relationship between the magnetic flux density generated by the permanent magnet and that generated by the electrode stub is obtained as shown in Equation (27).

$$\begin{aligned}\frac{1}{\mu_0\sigma}\left(\frac{\partial^2B_{n,z}}{\partial y\partial z} - \frac{\partial^2B_{n,y}}{\partial z^2}\right) &= v_y\left(\frac{B_{n,z}}{\partial z} + \frac{B_{e,z}}{\partial z}\right), \frac{1}{\mu_0\sigma}\left(\frac{\partial^2B_{n,z}}{\partial x\partial z} - \frac{\partial^2B_{n,x}}{\partial z^2}\right)\\ &= 0, \frac{1}{\mu_0\sigma}\left(\frac{\partial^2B_{n,y}}{\partial x\partial z} - \frac{\partial^2B_{n,x}}{\partial y\partial z}\right)\\ &= v_y\left(\frac{B_{n,x}}{\partial z} + \frac{B_{e,x}}{\partial z}\right)\end{aligned} \tag{27}$$

The pressures are calculated from the Navier–Stokes equation and Lorentz force. The force density of the MHD circulation system can be calculated as Equation (28) from the vector product of the current density in Equation (26) and the magnetic flux density in Equations (8)-(10). The y-direction of the force is necessary to create pressure in the MHD circulation system. Therefore, the z- and x-directions of magnetic flux density and *x*-direction of the electric field are the only factors we consider. The force due to electromotive is defined as the disturbed force for developing pressure in Equation (29), and the Lorentz force is defined in Equation (30) [11].

$$\begin{aligned}\vec{f} = \vec{J}_t\times\vec{B}_t = &\{\sigma E_y(B_{n,z} + B_{e,z}) - \sigma(v_yB_{n,x} - v_yB_{e,x})(B_{n,y} + B_{e,y})\}\hat{x}\\ &+\{\sigma(E_x + v_yB_{n,z} + v_yB_{e,z})(B_{n,z} + B_{e,z}) - \sigma(v_yB_{n,x} + v_yB_{e,x})(B_{n,x} + B_{e,x})\}\hat{y}\\ &+\{\sigma(E_x + v_yB_{n,z} + v_yB_{e,z})(B_{n,y} + B_{e,y}) - \sigma E_y(B_{n,x} + B_{e,x})\}\hat{z}\end{aligned} \tag{28}$$

$$f_E = -\sigma(v_yB_{n,x} + v_yB_{e,x})(B_{n,x} + B_{e,x}) \tag{29}$$

$$f_L = \sigma(E_x + v_yB_{n,z} + v_yB_{e,z})(B_{n,z} + B_{e,z}) \tag{30}$$

The Navier–Stokes equation in Equation (5) is represented in a dimensionless form in Equation (31) with dimensionless variables.

$$\frac{\partial\vec{v^*}}{\partial t^*} + \left(\vec{v^*}\cdot\nabla^*\right)\vec{v^*} = -\nabla^*\left(\vec{p^*} + \vec{p_h^*}\right) + \frac{N}{H_a^2}\nabla^{*2}\vec{v^*} + N\left(\vec{J_t^*}\times\vec{B}\right) \tag{31}$$

where

$$H_a = BL\sqrt{\frac{\sigma}{\rho\nu}}$$

$$N = \frac{\sigma LB^2}{\rho\nu}$$

$$p\rightarrow p^*\rho v^2$$

$$p_h\rightarrow p_h^*\rho v^2$$

$$v\rightarrow v^*v$$

$$t\rightarrow t^*\frac{L}{v}$$

$$j\rightarrow j^*\sigma vB$$

$$B\rightarrow B^*B$$

$$\nabla\rightarrow\nabla^*\frac{1}{L}$$

The temporal term $(\frac{\partial\vec{v^*}}{\partial t^*})$ is 0 for the steady state of the MHD circulation system. The liquid sodium, which is an incompressible fluid, satisfies Equations (32)-(33). Therefore, the convection term $(\vec{v^*}\cdot\nabla^*)\vec{v^*} = v_y^*\frac{\partial v_y^*}{\partial y}$ is also negligible.

$$\nabla\cdot v^* = 0 \tag{32}$$

$$\frac{\partial v_y^*}{\partial y} = 0 \tag{33}$$

The viscous term $\left(\frac{N}{Ha^2}\nabla^{*2}\vec{v^*}\right)$ is negligible when the Hartmann number is sufficiently high. The front term $(\frac{N}{Ha^2})$ is independent of the magnetic flux density $(=\frac{vL}{\nu})$, and the rear term $(\nabla^{*2}\vec{v^*})$ could be

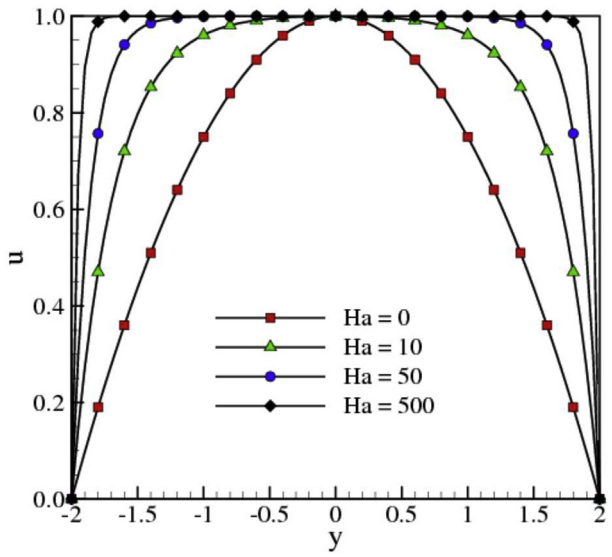


**Fig. 3.** Flow velocity profile at different values of the Hartmann number.

negligible because a high Hartmann number results in a flat velocity profile, the second-order differential of which is 0, as shown in Fig. 3 [12]. In the case of the MHD transportation system, a strong external magnetic field is applied to the fluid; therefore, the electromagnetic force is higher than the viscous force. Therefore, the viscous force is considered negligible in the MHD transportation system.

Accordingly, the Navier–Stokes equation is reduced to Equation (34) for the steady-state incompressible flow of liquid sodium, and it can be reduced to the parameters of pressure gradient, force density, and hydraulic pressure loss in Equation (34) [13,14].

$$\nabla p = \vec{J_t} \times \vec{B} - \nabla p_h \tag{34}$$

The hydraulic pressure loss $\Delta p_h$ is calculated from the Darcy–Weisbach formula in Equation (35), where the Darcy friction coefficient for turbulent flow $f_d$ is given by Equation (36) [15].

$$\Delta \mathrm{p_h} = \frac{\mathrm{f_d}\rho \mathrm{L} v^2 (\mathrm{W_d} + \mathrm{H_d})}{4 \mathrm{W_d} \mathrm{H_d}} \tag{35}$$

$$\frac{1}{\sqrt{\mathrm{f_d}}} = -1.8 \log_{10}\left[\frac{6.9}{\mathrm{Re}} + \left(\frac{\varepsilon_s}{3.7\mathrm{D}}\right)^{1.11}\right] \tag{36}$$

By combining Equations (27)-(36), the developed pressure is obtained as Equation (37).

$$\Delta \mathrm{p} = \int \{\sigma(E_x + v_y B_{n,z} + v_y B_{e,z})(B_{n,z} + B_{e,z})\} \mathrm{dV} - \sigma(v_y B_{n,x} - v_y B_{e,x})(B_{n,x} + B_{e,x}) \Big\} dy - \frac{\mathrm{f_d}\rho \mathrm{L} v_z^2 (\mathrm{W_d} + \mathrm{H_d})}{4 \mathrm{W_d} \mathrm{H_d}} \tag{37}$$

Equation (33) is used for calculating the total developed pressure, which is 2 kPa at a flow rate of 0.02 $m^3/s$, to consider the electric field from current, the magnetic flux density from the electrode stub and permanent magnet, and the geometrical variables that affect the resistance and hydraulic variables.

The finite element method (FEM) is used for calculating the electromagnetic conditions of the MHD circulation system through a simulation based on ANSYS code. Maxwell's equations and the Navier–Stokes equation could be represented as Equations (38)-(50) at three-dimensional nodes.

$$\frac{\partial \mathrm{B}_{\mathrm{n,z}}^{i,j,k}}{\partial y} - \frac{\partial \mathrm{B}_{\mathrm{n,y}}^{i,j,k}}{\partial z} = \mu_0 J_x^{i,j,k} \tag{38}$$

$$\frac{\partial \mathrm{B}_{\mathrm{n,x}}^{i,j,k}}{\partial z} - \frac{\partial \mathrm{B}_{n,z}^{i,j,k}}{\partial x} = \mu_0 J_y^{i,j,k} \tag{39}$$

$$\frac{\partial \mathrm{B}_{\mathrm{n,y}}^{i,j,k}}{\partial x} - \frac{\partial \mathrm{B}_{\mathrm{n,x}}^{i,j,k}}{\partial y} = \mu_0 J_z^{i,j,k} \tag{40}$$

$$\frac{\partial \mathrm{E}_{\mathrm{z}}^{i,j,k}}{\partial y} - \frac{\partial \mathrm{E}_{\mathrm{y}}^{i,j,k}}{\partial z} = 0 \tag{41}$$

$$\frac{\partial \mathrm{E}_{\mathrm{x}}^{i,j,k}}{\partial z} - \frac{\partial \mathrm{E}_{\mathrm{z}}^{i,j,k}}{\partial x} = 0 \tag{42}$$

$$\frac{\partial \mathrm{E}_{\mathrm{y}}^{i,j,k}}{\partial x} - \frac{\partial \mathrm{E}_{\mathrm{x}}^{i,j,k}}{\partial y} = 0 \tag{43}$$

$$\frac{\partial B_x^{i,j,k}}{\partial x} + \frac{\partial B_y^{i,j,k}}{\partial y} + \frac{\partial B_z^{i,j,k}}{\partial z} = 0 \tag{44}$$

$$\mathrm{J}_x^{i,j,k} = \sigma\left(E_x^{i,j,k} + v_y^{i,j,k} B_z^{i,j,k}\right) \tag{45}$$

$$\mathrm{J}_y^{i,j,k} = \sigma\left(E_y^{i,j,k}\right) \tag{46}$$

$$\mathrm{J}_z^{i,j,k} = \sigma\left(E_z^{i,j,k} - v_y^{i,j,k} B_x^{i,j,k}\right) \tag{47}$$

$$\frac{1}{\rho}\frac{\partial\left(p_x^{i,j,k} + p_{h,x}^{i,j,k}\right)}{\partial x} = \frac{1}{\rho}\left(J_y^{i,j,k} B_z^{i,j,k} - J_z^{i,j,k} B_y^{i,j,k}\right) \tag{48}$$

$$\frac{1}{\rho}\frac{\partial\left(p_y^{i,j,k} + p_{yh,}^{i,j,k}\right)}{\partial y} = \frac{1}{\rho}\left(J_z^{i,j,k} B_x^{i,j,k} - J_x^{i,j,k} B_z^{i,j,k}\right) \tag{49}$$

$$\frac{1}{\rho}\frac{\partial\left(p_z^{i,j,k} + p_{h,z}^{i,j,k}\right)}{\partial z} = \frac{1}{\rho}\left(J_x^{i,j,k} B_y^{i,j,k} - J_y^{i,j,k} B_x^{i,j,k}\right) \tag{50}$$

The nodes (i,j,k) are calculated based on Maxwell's equations and the Navier–Stokes equation. The current density, magnetic flux

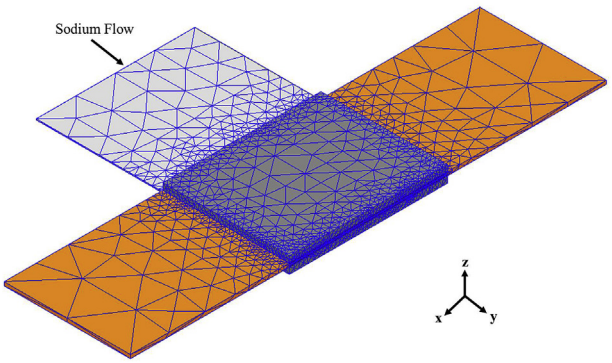


**Fig. 4.** Computational meshing of the rectangular-type MHD circulation system.

density, and velocity are obtained from Equations (38)-(50) in the simulation based on ANSYS code. The negligible terms are used for the increment of calculating speed of the code. The calculated values are used to analyze MHD values to drive the circulation system.

## 3. Results and discussion

Current in the MHD circulation system passed from the electrode stub to the system duct, which was comprised of 316L stainless steel, which was selected for its low reactivity with sodium [16]. The system then branched out to the permanent magnet, liquid sodium, and system duct. The permanent magnet ($Sm_2CO_{17}$) is used for generating the magnetic flux density because it generates a higher magnetic flux compared to the Alnico magnet in a high-temperature condition. The electrical conductivity of the permanent magnet ($Sm_2CO_{17}$) was 17% ($1.1 \times 10^6$ S/m) of that of the liquid sodium. The current could leak to the permanent magnet when the permanent magnet was attached to the system duct. Therefore, an insulating material was adopted between the

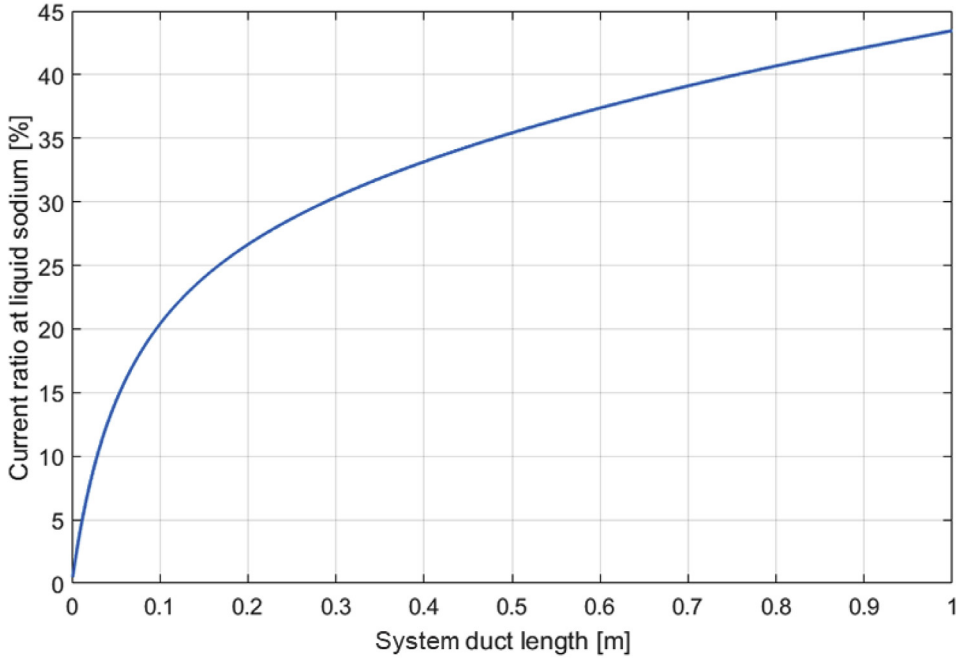


**Fig. 5.** Current ratio at liquid sodium according to system duct length at system duct height = 0.017 m

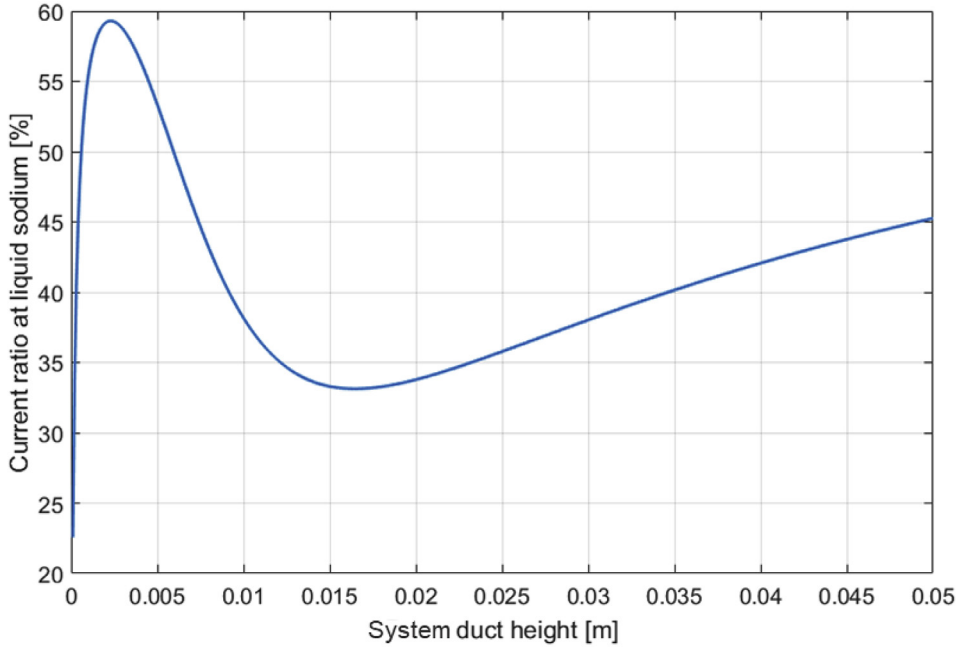


**Fig. 6.** Current ratio at liquid sodium according to system duct height at system duct length = 0.4 m

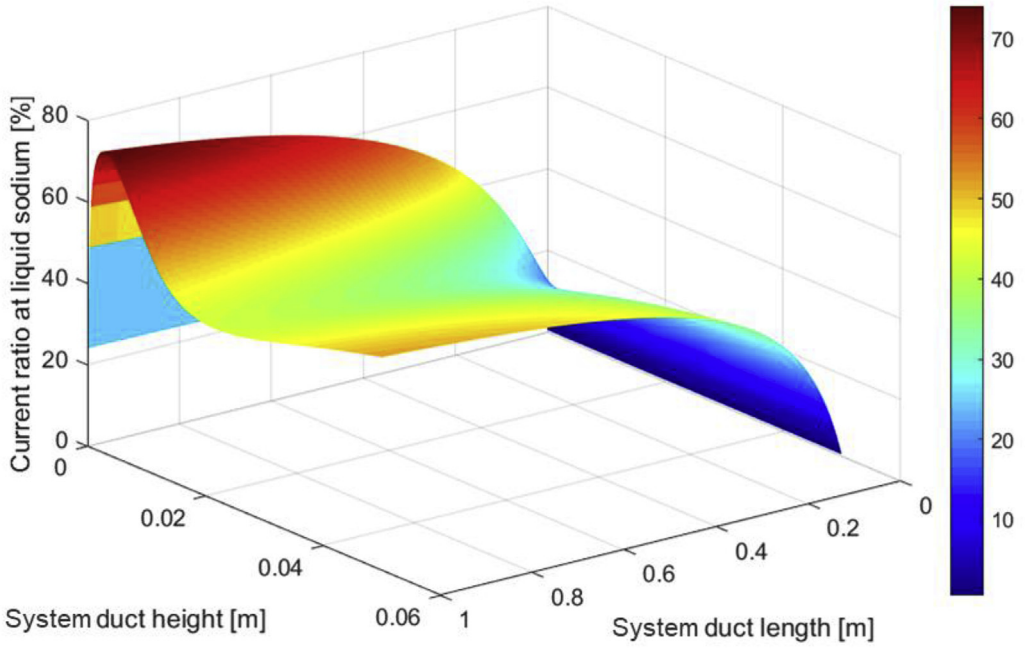


**Fig. 7.** 3-D plot current ratio at liquid sodium according to system duct height and system duct length.

permanent magnet and system duct, to minimize current loss in the liquid sodium, as shown in Fig. 2.

The current ratio in the liquid sodium—that is, the ratio of current flowing in the liquid sodium to the input current, was an important factor in analyzing the Lorentz force pressure, because it directly affected the current flowing in the liquid sodium. The computational meshing for calculating the current ratio is depicted in Fig. 4. The system duct resistance and fluid velocity were dominant factors determining the current ratio. As the system duct length increased, the resistance of the system duct increased more than that of the sodium because the system duct is surrounded by the liquid sodium. Therefore, the current ratio increased as the system duct length increased, as shown in Fig. 5.

The current ratio as a function of the system duct height is shown in Fig. 6. The current ratio rapidly increases up to a system duct height of 0.002 m because the system duct height affects velocity, which force due to electromotive. The very small system duct height (<0.02 m) causes very high velocities at a constant flow rate. The high velocity causes high force due to the electromotive force. Therefore, the current ratio increases as the system duct height increases because of the diminishing force due to the electromotive. As the system duct length increases from 0.002 m to

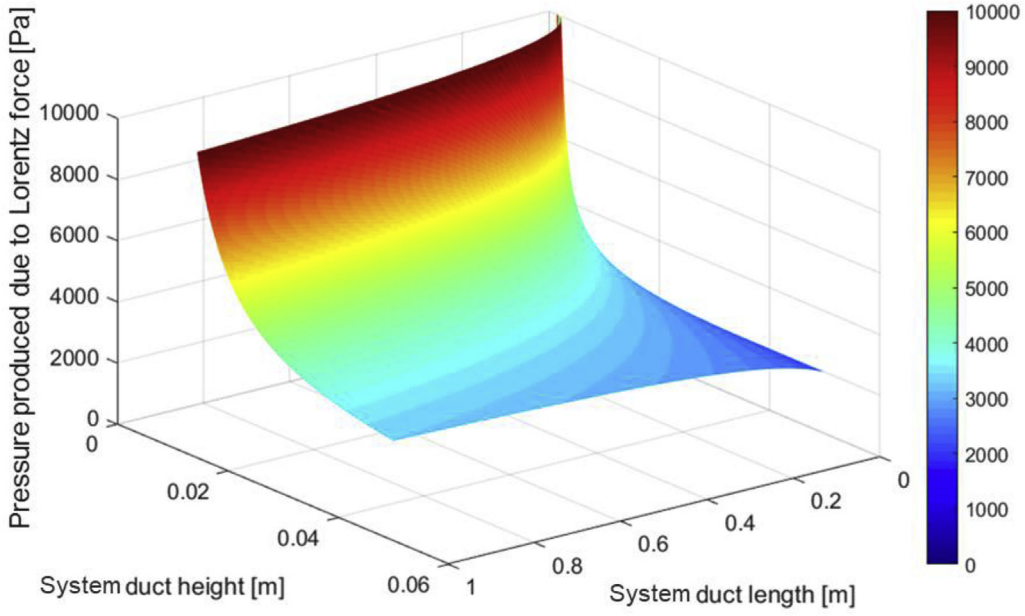


**Fig. 8.** 3-D plot pressure due to Lorentz force according to system duct height and system duct length.

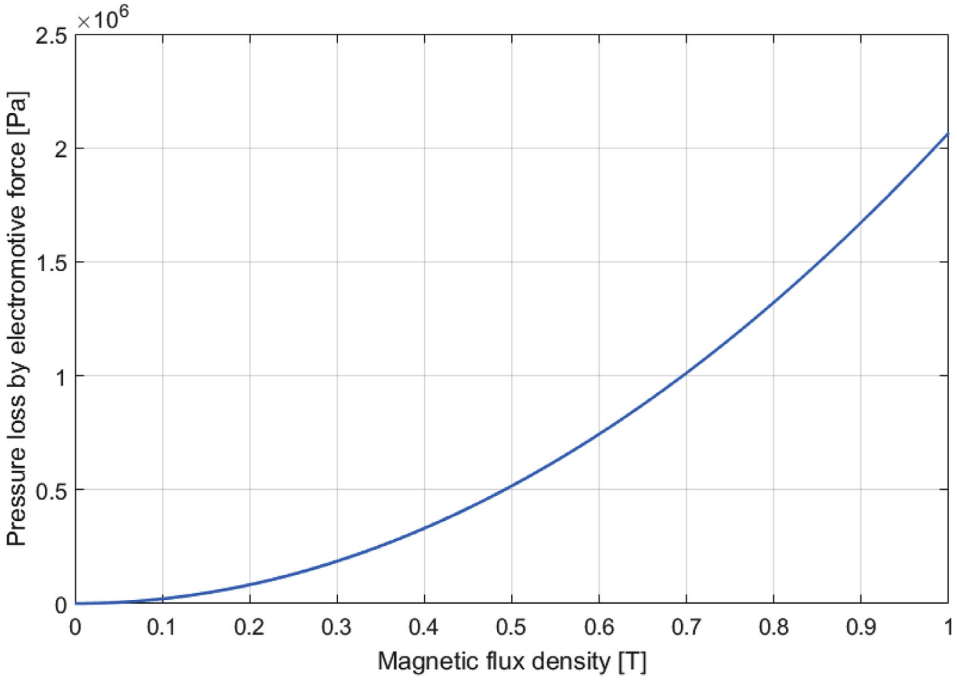


**Fig. 9.** Pressure loss by electromotive force according to magnetic flux density.

0.017 m, the current ratio decreases, because the increased system duct resistance is higher than that of sodium. The current increased more at the system duct than at liquid sodium with increasing system duct length. When the system duct is longer than 0.017 m, the velocity effects are higher than the resistance effects. Consequently, the current ratio increases.

A three-dimensional plot of the current ratio in the liquid sodium as a function of system duct height and length is shown in Fig. 7. The pressure produced by the Lorentz force was calculated using the current ratio for the liquid sodium. The pressure calculation was based on Equation (33), which represents an inverse proportion to the system duct height. Therefore, the tendency of the pressure produced by the Lorentz force follows the current ratio divided by the system duct height represented in Fig. 8. In the case of force due to electromotive, it follows a quadratic function with respect to the magnetic flux density described in Equation (33) and shown in Fig. 9. The force due to electromotive is proportional to the square of the magnetic flux density. The tendency of pressure loss with force due to electromotive according to the system geometry is shown in Fig. 10. As the system duct height increases, the force due to electromotive decreases, because of the increased velocity.

Meanwhile, the system duct length has a small effect on force due to electromotive compared to the system duct height.

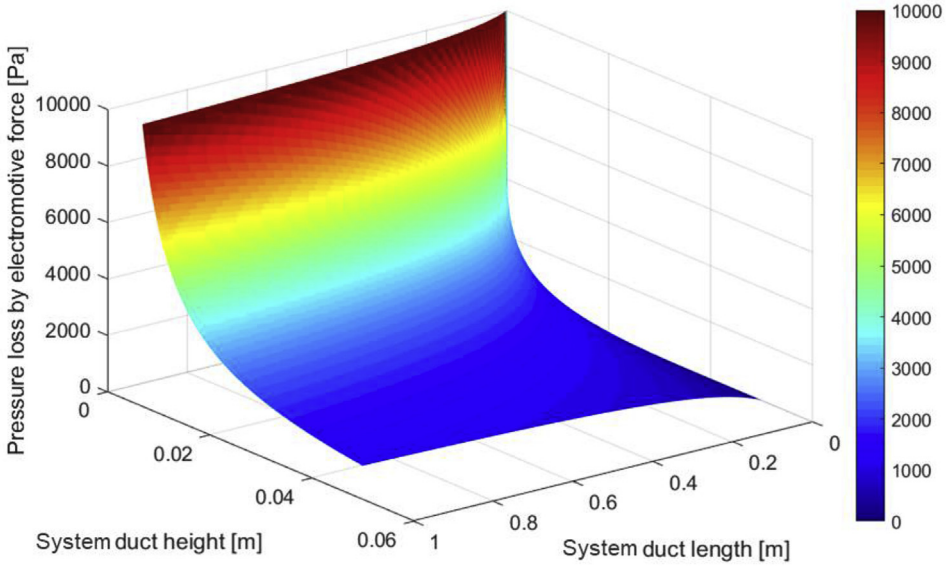


**Fig. 10.** 3-D plot pressure loss by electromotive force according to system duct height and system duct length.

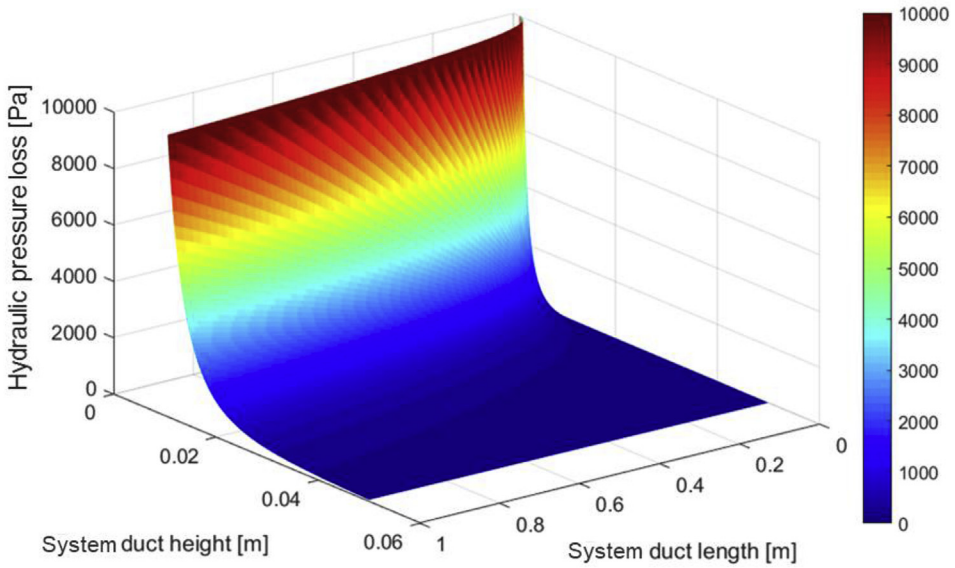


**Fig. 11.** 3-D plot pressure by hydraulic according to system duct height and system duct length.

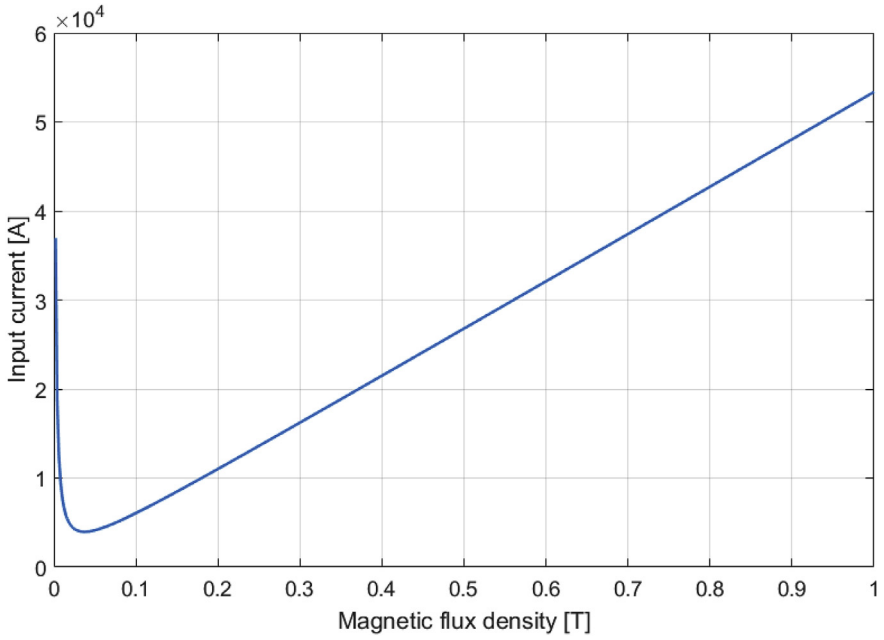


**Fig. 12.** Input current according to magnetic flux density at system duct height = 0.017 m and system duct length = 0.4 m.

Hydraulic pressure loss mainly affects system duct height because it depends on the velocity of the liquid sodium, as represented as Fig. 11. The magnetic flux density affects the input current because it influences both the Lorentz force and force due to the electromotive. In the low magnetic flux density (>0.3 T) condition, the Lorentz force, which is proportional to the magnetic flux density, is low. The high input current is needed to satisfy the developed pressure at low magnetic flux density condition. In the high magnetic flux density (<0.3 T) condition, the force due to the electromotive is a dominant factor because the Lorentz force is sufficient. Therefore, the input current is minimized, as shown in Fig. 12, which has a value of 3976 A at 0.037 T of the magnetic flux density. Fig. 13 shows the input current as a function of system duct geometry. In Table 1, the design specification of the MHD circulation system shows the optimized geometrical values of a system duct of length 0.4 m and height 0.017 m for achieving the minimized input current of 3976 A. The Hartmann number of the MHD circulation system is 1,858, which indicates that the viscous term could be negligible ($H_a \gg 1$).

## 4. Conclusion

We analyzed a rectangular-type MHD circulation system for use as an ADHRS in PGSFR by considering the current and magnetic flux density from the MHD equations. The current ratio was used to calculate the pressure in the MHD circulation system, and the

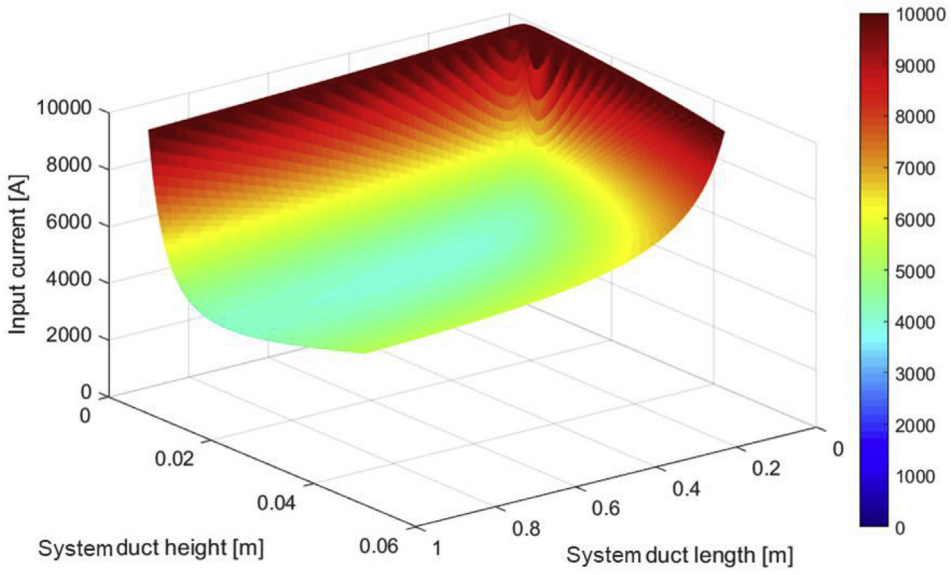


**Fig. 13.** 3-D plot input current according to system duct height and system duct length.

**Table 1**
Design specifications of the MHD circulation system.

| | Design variables | Unit | Values |
|---|---|---|---|
| Hydrodynamic | Flow rate ($Q$) | [$m^3/s$] | 0.02 |
| | Developed pressure ($\Delta P$) | [kPa] | 2 |
| | Temperature ($T$) | [K] | 499 |
| | Velocity ($v$) | [m/s] | 2.4 |
| | Reynolds number ($R_e$) | | $1.7 \times 10^5$ |
| | Pressure produced due to Lorentz force ($\Delta P_L$) | [kPa] | 5.69 |
| | Pressure loss due to EMF ($\Delta P_E$) | [kPa] | 2.83 |
| | Hydraulic pressure loss ($\Delta P_H$) | [kPa] | 0.86 |
| Geometrical | Height ($H_d$) | [m] | 0.017 |
| | Width ($W_d$) | [m] | 0.5 |
| | Length ($L$) | [m] | 0.4 |
| | Thickness ($t_h$) | [m] | 0.001 |
| Electromagnetic | Conductivity of permanent magnet | [1/(Ω·m)] | $1.1 \times 10^6$ |
| | Conductivity of system duct | [1/(Ω·m)] | $9.4 \times 10^5$ |
| | Conductivity of liquid sodium | [1/(Ω·m)] | $6.4 \times 10^6$ |
| | Input current ($i_t$) | [A] | 3976 |
| | Magnetic flux density ($B$) | [T] | 0.037 |
| | Voltage | [V] | 0.059 |
| | Efficiency | [%] | 17 |

magnetic flux density was optimized to minimize input current. We derived a minimized current of 3976 A and optimized magnetic flux density of 0.037 T. We believe that the required conditions of a developed pressure of 2 kPa and a flow rate of 0.02 $m^3/s$ can be satisfied with these optimized geometrical variables.

## Acknowledgments

This work was supported by the Korea Electric Power Corporation (Grant number : R18XA06-26) and National Research Foundation of Korea (NRF) grant funded by the Korean government (NRF-2016M2B2A9A02944010).

## Nomenclature

| | |
|---|---|
| B | Magnetic flux density [T] |
| $B_e$ | Magnetic flux density of permanent magnet [T] |
| $B_i$ | Magnetic flux density of electrode stub [T] |
| $B_t$ | Total magnetic flux density [T] |
| $D$ | Hydraulic diameter [m] |
| E | Electric field [kg.m/($s^3$·A)] |
| $E_t$ | Total electric field [kg.m/($s^3$·A)] |
| f | Force density [kg/($s^2$·$m^2$)] |
| $f_d$ | Darcy friction factor |
| $f_E$ | Force due to electromotive [kg/($s^2$·$m^2$)] |
| $f_L$ | Lorentz force [kg/($s^2$·$m^2$)] |
| H | Magnetic field intensity [A/m] |
| $H_a$ | Hartmann number |
| $H_d$ | System duct height, except for wall thickness [m] |
| $H_m$ | Magnetic field intensity of permanent magnet [A/m] |
| J | Current density [$A/m^2$] |
| $J_t$ | Total current density [$A/m^2$] |
| $L$ | Length of the system duct [m] |
| M | Magnetization [A/m] |
| N | Interaction parameter |
| p | Developed pressure of the system [Pa] |
| $p_h$ | Hydraulic pressure loss in the system [Pa] |
| Re | Reynolds number |

| | |
|---|---|
| t | Time [s] |
| $t_h$ | Thickness of the system duct [s] |
| v | Velocity of the fluid [m/s] |
| $W_d$ | System duct width, except for wall thickness [m] |
| $\varepsilon_0$ | Permittivity in vacuum [F/m] |
| $\mu_0$ | Permeability in vacuum [H/m] |
| $\mu_r$ | Relative permeability |
| $\nu$ | Kinematic viscosity [$m^2/s$] |
| $\rho$ | Density of liquid metal [$kg/m^3$] |
| $\rho'$ | Resistivity of liquid metal [$\Omega \cdot m$] |
| $\sigma$ | Electrical conductivity of liquid metal [$1/(\Omega \cdot m)$] |
| $\chi_m$ | Magnetic susceptibility |

## References


[1] A.U. Gutierrez, C.E. Heckathorn, Electromagnetic Pumps for Liquid Metals, Naval Postgraduate School, California, 1965.

[2] D. Kim, J. Hong, T. Lee, Design of DC Conduction Pump for PGSFR Active Decay Heat Removal System, Transactions of the Korean Nuclear Society Spring Meeting, Korea, 2014.

[3] L.R. Blake, Conduction and induction pumps for liquid metals, Proc. IEE-Part A: Power Eng. 104 (13) (1957) 49–67.

[4] C. Wagner, Theoretical analysis of the current density distribution in electrolytic cells, J. Electrochem. Soc. 98 (3) (1951) 116–128.

[5] T. Oka, N. Kawasaki, S. Fukui, J. Ogawa, T. Sato, T. Terasawa, Y. Itoh, R. Yabuno, Magnetic field distribution of permanent magnet magnetized by static magnetic field generated by HTS bulk magnet, IEEE Trans. Appl. Supercond. 22 (3) (2012) 9502304.

[6] M. Hughes, K.A. Pericleous, M. Cross, The Numerical modelling of DC electromagnetic pump and brake flow, Appl. Math. Model. 19 (12) (1995) 713–723.

[7] R.S. Baker, M.J. Tessier, Handbook of Electromagnetic Pump Technology, Elsevier, New York, 1987.

[8] B.K. Nashine, S.K. Dash, K. Gurumurthy, M. Rajan, G. Vaidyanathan, Design and testing of DC conduction pump for sodium cooled fast reactor, in: 14th International Conference on Nuclear Engineering, American Society of Mechanical Engineers (ASME), 2006.

[9] G.H. Lee, H.R. Kim, Numerical investigation and comparison of the rectangular, cylindrical, and helical-type DC electromagnetic pumps, Magnetohydrodynamics 53 (2) (2017) 429–438.

[10] D.A. Watt, The design of electromagnetic pumps for liquid metals, Proc. IEE-Part A: Power Eng. 106 (26) (1959) 94–103.

[11] N. Bennecib, S. Drid, R. Abdessemed, Numerical investigation of flow in a new DC pump MHD, J. Appl. Fluid Mechan. 2 (2) (2009) 23–28.

[12] W.K. Hussam, M.C. Thompson, G.J. Sheard, Quasi-2D Simulation of Liquid Metal Flow Past a Cylinder in a Duct Exposed to a Magnetic Field, Australasian Fluid Mechanics Conference, New Zealand, 2010.

[13] R.W. Ohse, Handbook of Thermodynamic and Transport Properties of Alkali Metals, Blackwell Scientific, Oxford, 1985.

[14] B.K. Nashine, S.K. Dash, K. Gurumurthy, U. Kale, V.D. Sharma, R. Prabhaker, M. Rajan, G. Vaidyanathan, Performance testing of indigenously developed DC conduction pump for sodium cooled fast reactor, Indian J. Eng. Mater. Sci. 14 (2007) 209–214.

[15] Crane Co (US), Flow of Fluids through Valves, Fittings, and Pipe, Crane Co., Chicago (IL), 1977. Technical Paper No. 410.

[16] C.Y. Ho, T.K. Chu, Electrical resistivity and thermal conductivity of nine selected AISI stainless steels, CINDAS Rep. 45 (1977). Washington.